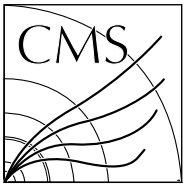

The Compact Muon Solenoid Experiment

CMS Note

Mailing address: CMS CERN, CH-1211 GENEVA 23, Switzerland

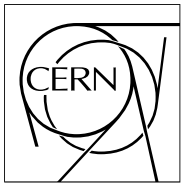

1 April 2006

Search for Randall-Sundrum excitations of gravitons decaying into two photons for CMS at LHC

M.-C. Lemaire[1)], V. Litvin[2)], H. Newman[2)]

Abstract

The CMS detector discovery potential to the resonant production of massive Kaluza - Klein excitations expected in the Randall-Sundrum Model is studied. Full simulation and reconstruction are used to study diphoton decay of Randall-Sundrum gravitons. For an integrated luminosity of 30 fb^{-1} diphoton decay of Randall-Sundrum gravitons can be discovered at 5σ level for masses up to 1.61 TeV/c^2 in case of weak coupling between graviton excitations and Standard Model particles ($c = 0.01$). Heavier resonances can be detected for larger coupling constant ($c = 0.1$), with mass reach of 3.95 TeV/c^2.

[1)] SPP/DAPNIA, bat.141, CE Saclay, 91191 Gif-sur-Yvette France

[2)] California Institute of Technology, Pasadena, CA 91125, USA

1 Introduction

Several attempts to solve the hierarchy problem using extra spatial dimensions have been developed recently [1, 2, 3]. First, Arkani-Hamed, Dvipoulos and Dvali (ADD) [1], introduced large extra dimensions (compared to string scale) in order to create an extra volume which is sufficiently large to dilute gravity so that it appears weak for a 3D observer. Then, Randall and Sundrum (RS) [2] offered a rigorous solution of the hierarchy problem by adding a single extra dimension (with the size that can range from about $1/\bar{M}_{pl}$ to infinity) with a non Euclidean warped metric.

From the experimental point of view, only two parameters govern the RS model: M, the mass of the first Kaluza-Klein (KK) excitation of the graviton (RS-1), and a dimensionless parameter $c = k/\bar{M}_{pl}$, which governs the coupling of the graviton to the SM fields and hence define the natural width of the first KK graviton. The LHC can probe the full allowed range for these parameters [4].

The most recent experimental constraint [5] comes from the D0 experiment at FNAL Tevatron, which does not distinguish electrons from photons thus calling them "EM objects". The D0 Collaboration excludes M_G up to 250 $\mathrm{GeV/c^2}$ for c=0.01 and 785 $\mathrm{GeV/c^2}$ for c=0.1. The CDF Collaboaration [6, 7] provides the 95% CL limits separately in the three channels: dimuons, dielectrons and diphotons. The sensitivity is dominated by the diphoton channel not only due to higher statistics, but also due to the fact that branching fraction of RS graviton into diphotons is twice as large as that into a single dilepton channel [7].

LHC will provide a new opportunity window to detect Randall-Sundrum (RS) gravitons with higher resonance masses both for the weak coupling constant $c = 0.01$ as well as for the stronger $c = 0.1$. The sensitivity of CMS for the search of RS gravitons decaying into electron pairs is discussed in Ref. [8]. For an integrated luminosity of 100 $\mathrm{fb^{-1}}$, resonances can be discovered at 5σ level for masses up to 1.8 TeV/c^2 for c=0.01. Heavier resonances are accessible for larger values of the c parameter, with a mass reach of 3.8 TeV/c^2 for c=0.1. The detection of a resonance in the diphoton channel, in addition to e^+e^- and $\mu^+\mu^-$ channels, will present an evidence that this resonance is RS graviton, or any other particle with spin 0 or 2. It will exclude large number of models where large resonances with spin 1 does exist, like Z', for example, because Z' has spin 1 and cannot decay in two photons. Such obervation might occur before having accumulated the large amount of data needed to analyze the angular distributions in the dilepton channels.

The Note is organized as follows. Section 2 is dedicated to the event generation and kinematic preselection. The offline selection and the analysis is discussed in Section 3, K-factors are briefly discussed in Section 4 and final results are presented and discussed in Section 5.

2 Event generation and kinematics preselection

The generation of proton-proton collisions at 14 TeV centre of mass energy is done with PYTHIA 6.227 [9], which takes into account the angular distributions of the RS process decaying into two photons. The datasets produced cover all region of interest in the (M_G, c) space (Fig. 1).

At parton level, single gravitons can be produced via $q\bar{q} \to G$ and $gg \to G$. The cross-sections for these processes are displayed in Fig. 2 (left). The lorentzian width of the RS resonance (Γ) varies with M_G and c as illustrated in Fig. 2 (right). As an example, for a RS-1 graviton mass M_G = 1.5 TeV/c^2, the lorentzian resonance width varies from 0.20 GeV/c^2 for $c = 0.01$ to 19 GeV/c^2 for $c = 0.1$.

The CTEQ5L parton distribution set of Ref. [10] has been chosen. The influence of parton distribution function choice will be taken into account as systematic uncertainties and will be discussed in Section 6.

The search for the G $\to \gamma\gamma$ signal at LHC is affected by four types of backgrounds:

- The prompt di-photon production from the quark annihilation (Table 1) and gluon fusion (Table 2) diagrams, which provides an intrinsic or 'irreducible' background.
- The γ + jets production consisting of two parts: i) prompt photon from hard interaction plus the second photon coming from the outgoing quark due to initial and final state radiation and ii) prompt photon from hard interaction plus the decay of a neutral hadron (mostly isolated π^0) in a jet, which could fake a real photon (Table 3).
- The background from QCD hadronic jets, where electromagnetic energy deposits result from the decay of neutral hadrons (especially isolated π^0s) in both jets (Table 4).

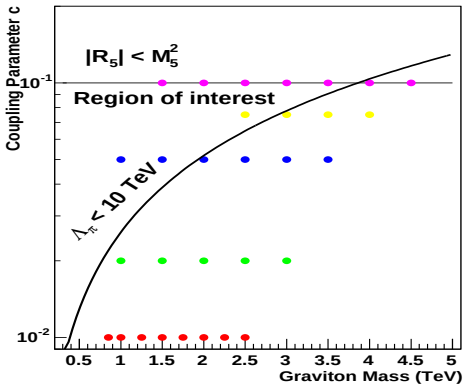

Figure 1: Signal coverage of the region of interest for RS graviton diphoton decay study.

- Drell Yan process with e^+e^- in a final state which could mimic photons when correspondent electron tracks will not be assigned to the superclusters during the reconstruction (Table 5).

2.1 QCD hadronic jets and γ+jets generator level preselection

A preselection at generator level has been developed. Its aim is to select only events which can be measured in the detector as two isolated photons.

First, all particles which will produce large energy deposit in the ECAL are identified. Then, around each of these particles, a search is performed to find in a narrow cone all the less energetic particles, which are also able to deposit energy in the ECAL and thus will be reconstructed as a parts of the same Super-Cluster. Each family of these particles gives a "Super-Cluster candidate". A loose tracker isolation is also performed: it requests that in a cone $\Delta R = 0.2$ around each "Super-Cluster candidate" the number of charged particles is less or equal to three. The "Super-Cluster candidates" are ordered by decreasing energy. The total number of charged particles, in the two cones around the first and second one, must be less or equal to six. Kinematical cuts are also applied

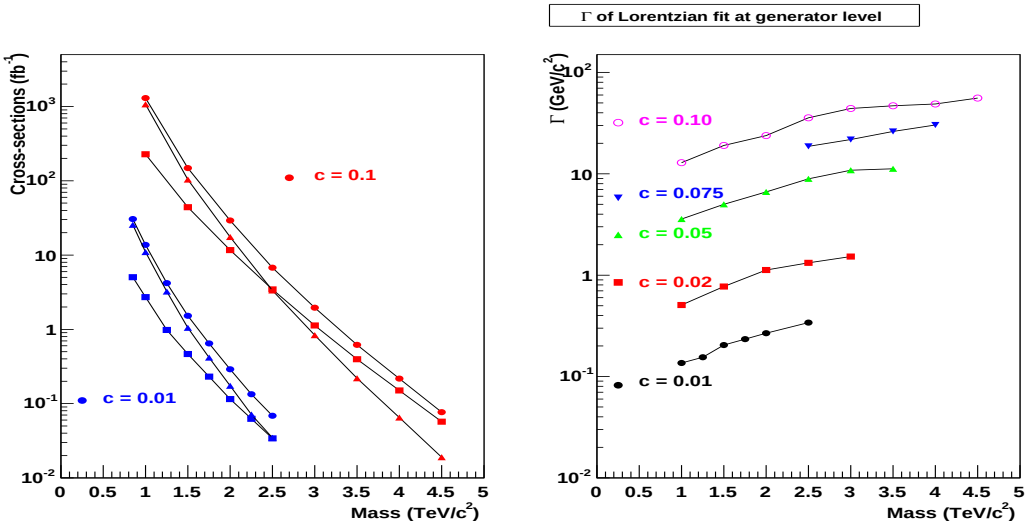

Figure 2: Parton level cross-sections (left) and lorentzian widths of RS-1 graviton resonances (right) for different mass M_G and coupling constants c. Square markers are for $q\bar{q}$ RS-1 graviton production, triangle markers are for gg RS-1 graviton production, circle markers are for the total cross-section.

Table 1: Datasets generated with PYTHIA for the simulation of the quark annihilation background. The Table contains the range of allowed $\hat{m} = \sqrt{\hat{s}}$ values for the subprocesses; the corresponding PYTHIA cross-section (σ_{PYTHIA}); the rejection factor r which is the ratio between the numbers of preselected and generated events; the cross-sections of the preselected process ($\sigma_{sel} = \sigma_{PYTHIA}/r$); the number of events generated in the relevant mass intervals.

Dataset	CKIN(1)-CKIN(2), TeV/c^2	σ_{PYTHIA}, fb	rejection rate r	σ_{sel}, fb	Nevents
Born	0.6-0.8	37.	1.56	23.72	2500
Born	0.8-1.3	20.25	1.582	12.8	4000
Born	1.3-1.9	3.31	1.69	1.96	2000
Born	1.9-3.2	0.75	1.84	0.407	1000
Born	3.2-5.25	0.043	2.19	0.0196	1000

Table 2: Datasets for the simulation of the gluon fusion background. The labels of the different columns are explained in the caption of Table 1.

Dataset	CKIN(1)-CKIN(2), TeV/c^2	σ_{PYTHIA}, fb	rejection rate r	σ_{sel}, fb	Nevents
Box	0.6-0.8	2.02	1.2	1.6	1000
Box	0.8-1.3	0.61	1.26	0.48	1000
Box	1.3-1.9	0.04	1.38	0.029	1000
Box	1.9-3.2	4.07*10^{-3}	1.42	2.9*10^{-3}	1000
Box	3.2-5.25	7.23*10^{-5}	1.62	4.46*10^{-5}	1000

Table 3: Datasets for the simulation of the γ+jets background. The labels of the different columns are explained in the caption of Table 1.

Dataset	CKIN(1)-CKIN(2), TeV/c^2	σ_{PYTHIA}, fb	rejection rate r	σ_{sel}, fb	Nevents
Brem	0.6-0.8	2.01*10^4	148.95	134.94	5k
Brem	0.8-1.3	8960	51.46	174.1	5k
Brem	1.3-1.9	1140.	40.69	28.	5k
Brem	1.9-3.2	210.	40.86	5.14	5k
Brem	3.2-5.25	9.7	37.19	0.26	5k
Brem	5.25-inf	0.144	31.512	0.0046	5k

Table 4: Datasets for the simulation of the QCD hadronic jets background. The labels of the different columns are explained in the caption of Table 1.

Dataset	CKIN(1)-CKIN(2), TeV/c^2	σ_{PYTHIA}, fb	rejection rate r	σ_{sel}, fb	Nevents
QCD	0.6-0.8	1.01*10^8	322471	310	20k
QCD	0.8-1.3	7.43*10^7	39049	1904	20k
QCD	1.3-1.9	1.9*10^7	12949	1467.3	20k
QCD	1.9-3.2	7.07*10^6	6116	1155.98	20k
QCD	3.2-5.25	9.56*10^5	2315	412.95	10k
QCD	5.25-inf	5.57*10^4	1244	44.77	5k

Table 5: Datasets for the simulation of the Drell-Yan background. The labels of the different columns are explained in the caption of Table 1.

Dataset	CKIN(1)-CKIN(2), TeV/c^2	σ_{PYTHIA}, fb	rejection rate r	σ_{sel}, fb	Nevents
DY	0.6-0.8	34.6	1.292	26.8	1000
DY	0.8-1.3	14.62	1.224	11.94	2500
DY	1.3-1.9	1.75	1.135	1.542	1500
DY	1.9-3.2	0.31	1.091	0.284	2500
DY	3.2-5.25	0.0125	1.036	0.012	1000

requiring that the first and second "Super-Cluster candidate" have their transverse momenta respectively above 150 and 100 $\mathrm{GeV/c}$ and their invariant mass must be above 550 $\mathrm{GeV/c^2}$.

First of all seed candidates are identified. Only the following particles, that can produce in the detector electromagnetic showers consistent with photons, are considered: γ, $\mathrm{e}^{\pm}$, π^0, η, η', ρ, ω.

The seeds must satisfy the cuts:

- $\mathrm{p_{t\,seed}} > \mathrm{p_{t\,seedmin}}$
- $|\eta_{\mathrm{seed}}| < \eta_{\mathrm{seedmax}}$

In order to take into account the fact that superclusters have a sizeable spread in η and ϕ and that more than one particle can contribute to the reconstructed energy these seeds are not used as photon candidates, but all final state γ and $\mathrm{e}^{\pm}$ around their direction are added. Thus a photon candidate is defined as the vector sum of all the γ and $\mathrm{e}^{\pm}$ momenta with the following selection:

- $\mathrm{p_{t\,\gamma}} > \mathrm{p_{t\,\gamma min}}$
- $|\eta_{\gamma}| < \eta_{\gamma \mathrm{max}}$
- $\mathrm{p_{t\,e}} > \mathrm{p_{t\,emin}}$
- $|\eta_{\mathrm{e}}| < \eta_{\mathrm{emax}}$
- $\Delta \mathrm{R} < \Delta \mathrm{R}_{\gamma-\mathrm{seed}}$ or ($\Delta\eta < \Delta\eta_{\gamma-\mathrm{seed}}$ and $\Delta\phi < \Delta\phi_{\gamma-\mathrm{seed}}$)

It is also possible to include $\mathrm{K^0_{long}}$ as seeds and as components of the candidate with the cuts:

- $\mathrm{p_{t\,K^0_{long}}} > \mathrm{p_{t\,K^0_{long}min}}$
- $|\eta_{\mathrm{K^0_{long}}}| < \eta_{\mathrm{K^0_{long}max}}$

In addition, the γ and $\mathrm{e}^{\pm}$ within a narrow cone around the seed are added in order to estimate the lowest possible energy that can be reconstructed for the candidate. These must satisfy.:

- $\mathrm{p_{t\,\gamma}} > \mathrm{p_{t\,\gamma min}}$
- $|\eta_{\gamma}| < \eta_{\gamma \mathrm{max}}$
- $\mathrm{p_{t\,e}} > \mathrm{p_{t\,emin}}$
- $|\eta_{\mathrm{e}}| < \eta_{\mathrm{emax}}$
- $\Delta \mathrm{R} < \Delta \mathrm{R}_{\mathrm{narrow}}$

This energy will be referred to as "narrow cone energy".

In order to evaluate the effect of the tracker isolation, stable or long lived charged particles around the direction of the photon candidates are counted using the following cuts:

Table 6: Signal datasets for RS graviton diphoton decay study. Mass and c are the model parameters described above, $\sigma_{q\bar{q}}$, σ_{gg}, σ_{tot} are the cross-sections to produce gravitons in quark annihilation, gluon fusion and total RS graviton production cross-section $\sigma_{tot} = \sigma_{q\bar{q}} + \sigma_{gg}$. Nevents is the total number of events produced.

Mass, TeV/c^2	c	σ_{tot}, fb	$\sigma_{q\bar{q}}$, fb	σ_{gg}, fb	Nevents
1.5	0.1	148.3	44.3	104	1000
2.0	0.1	29.2	11.6	17.6	1000
2.5	0.1	6.77	3.44	3.33	1000
3.0	0.1	1.96	1.13	0.835	1000
3.5	0.1	0.62	0.40	0.22	10000
4.0	0.1	0.217	0.152	0.065	1000
4.5	0.1	0.076	0.057	0.019	1000
2.5	0.075	3.85	2.0	1.85	1000
3.0	0.075	1.10	0.64	0.46	1000
3.5	0.075	0.35	0.23	0.13	1000
4.0	0.075	0.12	0.084	0.036	1000
1.0	0.05	328	63.0	265.0	1000
1.5	0.05	37.7	11.6	26.1	1000
2.0	0.05	7.12	2.86	4.26	1000
2.5	0.05	1.73	0.90	0.83	1000
3.0	0.05	1.10	0.64	0.46	1000
3.5	0.05	0.16	0.1	0.06	1000
1.0	0.02	55.5	10.9	44.6	1000
1.5	0.02	5.94	1.78	4.16	1000
2.0	0.02	1.12	0.45	0.67	1000
2.5	0.02	0.28	0.14	0.14	1000
3.0	0.02	0.08	0.047	0.033	1000
0.85	0.01	30.6	5.0	25.6	1000
1.0	0.01	13.7	2.7	11.0	1000
1.25	0.01	4.19	0.98	3.21	1000
1.5	0.01	1.52	0.47	1.05	1000
1.75	0.01	0.65	0.23	0.42	1000
2.0	0.01	0.29	0.12	0.17	10000
2.25	0.01	0.13	0.06	0.07	1000
2.5	0.01	0.069	0.034	0.035	1000

- $\mathrm{p_{t\,tk}} > \mathrm{p_{t\,tkmin}}$
- $\Delta\mathrm{R} < \Delta\mathrm{R_{tkmax}}$
- $|\eta_{\mathrm{tk}}| < \eta_{\mathrm{tkmax}}$

Finally, it is required that at least a pair of candidate photons in the event satisfy:

- $\mathrm{p_{t\,1}} > \mathrm{p_{t\,1min}}$
- $\mathrm{p_{t\,2}} > \mathrm{p_{t\,2min}}$
- $\mathrm{N_{tkcone1}}, \mathrm{N_{tkcone2}} \leq \mathrm{N_{tkconemax}}$
- $\mathrm{N_{tkcone1}} + \mathrm{N_{tkcone2}} \leq \mathrm{N_{tksummax}}$
- $|\eta_1|, |\eta_2| < \eta_{\mathrm{candmax}}$
- Invariant mass of the pair $> \mathrm{M_{\gamma\gamma_{min}}}$
- Invariant mass of the pair (using the narrow cone energies) $< \mathrm{M_{\gamma\gamma_{max}}}$

Table 7: Cuts for the QCD and brem background preselections.

Variable	Cut value
$\mathrm{p_{t\,seedmin}(GeV)}$	20.
η_{seedmax}	2.6
$\mathrm{p_{t\,\gamma min}(GeV)}$	0.0
$\eta_{\gamma\mathrm{max}}$	2.8
$\mathrm{p_{t\,emin}(GeV)}$	2.0
η_{emax}	2.8
Use $\mathrm{K^0_{long}}$	Yes
$\mathrm{p_{t\,K^0_{long}min}(GeV)}$	1.0
$\eta_{\mathrm{K^0_{long}max}}$	2.8
$\Delta\phi_{\gamma-\mathrm{seed}}$	0.4
$\Delta\eta_{\gamma-\mathrm{seed}}$	0.15
$\mathrm{\Delta R_{\gamma-seed}}$	0.2
$\mathrm{\Delta R_{narrow}}$	0.02
$\mathrm{p_{t\,tkmin}(GeV)}$	1.6
η_{tkmax}	2.2
$\mathrm{\Delta R_{tkmax}}$	0.2
$\mathrm{p_{t\,1min}(GeV)}$	150.
$\mathrm{p_{t\,2min}(GeV)}$	100.
η_{candmax}	2.6
$\mathrm{N_{tkconemax}}$	3
$\mathrm{N_{tksummax}}$	6
$\mathrm{M_{\gamma\gamma\,min}(GeV)}$	550
$\mathrm{M_{\gamma\gamma\,max}(GeV)}$	14000

Preselection inefficiency will be less than 1% uncertainty in the inefficiency to preselect $\gamma + jet$ events and smaller than 2% uncertainty in the inefficiency to preselect QCD hadronic jet events. This 1-2% inefficiency will be for the inefficiency on the level of preselected events and it will be propagated to the 1-2% of correspondent cross-section uncertainites.

3 Offline selection and analysis

3.1 Event simulation and reconstruction

The crucial detector in this analysis is the Electromagnetic Calorimeter (ECAL). It consists of lead tungstate ($PbWO_4$) crystals. These crystals have short radiation ($X_0 = 0.89$ cm) and Moliere (2.2 cm) lengths, are fast (80% of the light is emitted within 25 ns) and radiation hard (up to 10 Mrad). The scintillation light is detected by Si avalanche photodiodes in the barrel region and vacuum phototriodes in the endcap region. The sensitivity of both the crystals and the APD response to temperature changes requires a temperature stability at the level of about 0.1^o C. The use of $PbWO_4$ crystals has thus allowed the design of a compact calorimeter that is fast with fine granularity. ECAL readout system is structured into sets of 5×5 crystals. In the barrel, these 5×5 crystal sets correspond to the trigger towers. In the endcaps, the size of trigger cells varies, in order to follow approximately a projectile geometry. The 5×5 readout cells are called supercrystals, they are divided into five 5-crystal, variable shaped, pseudo-strips. Several pseudo-strips combine into the towers. Towers are the main trigger primitive for the ECAL L1 trigger.

A detailed description of the CMS detector can be found elsewhere [11, 12]. The simulation package OSCAR version 3.6.5 [13] based on GEANT4 was used to describe the detector geometry and materials. This package also handles the particle propagation and interactions with the detector. The reconstruction is done with the CMS object-oriented reconstruction package ORCA version 8.7.1 [14]. This package handles all reconstruction tasks as well as the simulation of the detector response, the Level-1 trigger [11] and High Level Trigger [12]. All events have been simulated with low luminosity pile-up, which corresponds to 2*10^33 instantaneous luminosity.

The Level-1 double trigger has a 98.2 % efficiency for the channel under study. At Level 2.5 [12], the photon candidates are selected by requiring that there is no ECAL clusters matching with hits in the pixel detector. Both

two photon and relaxed two photon triggers are accepted, in order not to kill the photons having high rear leakage in the HCAL. The efficiency after this selection is 97.1 %. Relaxed stream allows for non-isolated L1 triggers. It was a way to increase the efficiency in the $H \rightarrow \gamma\gamma$ case. The photon triggers used in this analysis correspond to the di-photon HLT triggers of the CMS Trigger Menu as listed in Table 15-24 of the DAQ TDR [12].

3.2 Non-saturated high energy photons study

3.2.1 Event simulation and reconstruction

The simulation package OSCAR version 3.6.5 [13] based on GEANT 4 was used to describe the detector geometry and materials. This package also handles the particle propagation and interactions in the detector. The reconstruction was done with CMS object-oriented-reconstruction package ORCA version 8.7.1 [14]. Various transverse momenta and energies (Table 8) have been considered to cover the dynamic range needed for the exploration of the RS-1 graviton signals. The saturation problem of E_1, crystal with the highest energy deposition in a cluster, at 1.7 TeV will be discussed later on.

The different trigger levels have been described previously [11, 12]. At Level 2.5, the energy-weighted average impact point is propagated back to the nominal vertex point and hits are looked in the pixel detectors. If at least two pixel hits are found, the candidate is classified as an electron, otherwise it is classified as a photon.

Table 8: Number of generated single photon events.

P_t value	η range	Number of events
0.25 TeV/c	$\|\eta\| < 2.5$	6000
0.75 TeV/c	$\|\eta\| < 2.5$	6000
1.8 TeV/c	$\|\eta\| < 2.5$	6000

3.2.2 High energy photon reconstruction

The photon is reconstructed as an ECAL Super-Cluster using the "Hybrid algorihtm" in the barrel and the "Island algorithm" in the endcaps [15], within the fiducial regions:$|\eta| < 1.442$ or $1.566 < |\eta| < 2.5$. The energy loss in the preshower is taken into account for endcap Super-Cluster reconstruction. A correction based on the fraction of hadronic energy over electromagnetic energy (H/E) is applied to correct for the small energy loss from shower leakage beyond the ECAL (Fig. 3). Previous study of RS-1 graviton decaying into electron pair [8] had already shown the improvement of the energy resolution when such correction is taken into account. A slight dependence on η of the ratio of the measured Super-Cluster energy E_{SC} to the generated energy E_{true} is displayed in Fig. 4. In the barrel, at P_t = 0.25 TeV/c, where the shower is still well contained in the ECAL this variation amounts to 0.6%, as expected from the well known "umbrella" effect due to the calorimeter geometry. As in Ref. [8], a correction with 10 bins in η is applied to bring the E_{SC}/E_{true} ratio back to unity. Between 0.25 and 1.8 TeV/c, for each η these coefficients differ by less than 1% with P_t and therefore has been kept constant, equal to their values determined for P_t = 0.75 TeV/c.

3.2.3 Photon resolution

In the reconstruction algorithm [15] a depth $tmax$ is defined as the longitudinal center of gravity of the shower, and its optimal value varies logarithmically with the shower energy. To account for this energy dependence a parametrization is used: A(T0+log(E)) where A is the radiation length of lead tunstate (0.89 cm). It was necessary to retune T0 for the endcap with preshower, to get a single peak in the distribution of η position resolution. The best performance for such high energetic photons is obtained with T0 = 4.6 as shown in Fig. 5, it has to be compared to T0 = 2.4 found for low energy photons.

In such conditions the mean and sigma values of the gaussian fits of the position resolution distributions are given in Table 9 for the various P_t samples studied.

The energy resolution obtained by taking the energy deposit in a Super-Cluster is compared to that reached by using a 5 by 5 crystal matrix and presented in Fig. 6. The gaussian fits were performed, and σ_{eff}, defined as the half-width containing 68.3% of the distribution, have been estimated.

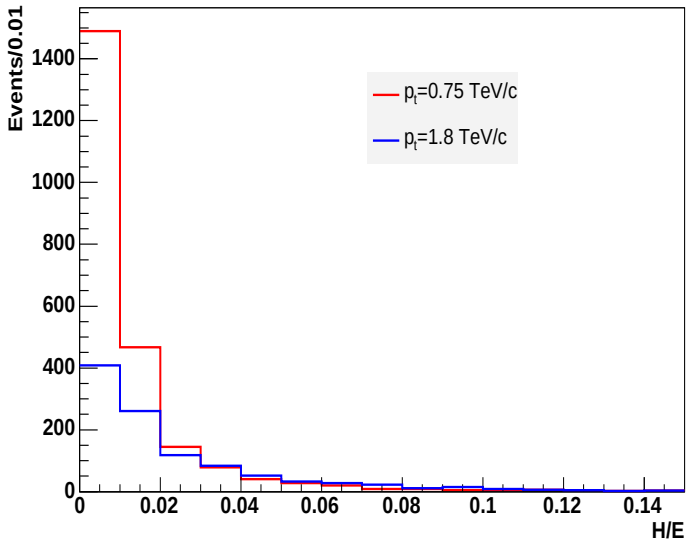

Figure 3: Hadronic to electromagnetic energies ratio (H/E) in the endcap for $\mathrm{P_t}$=0.75 and 1.8 TeV/c photons.

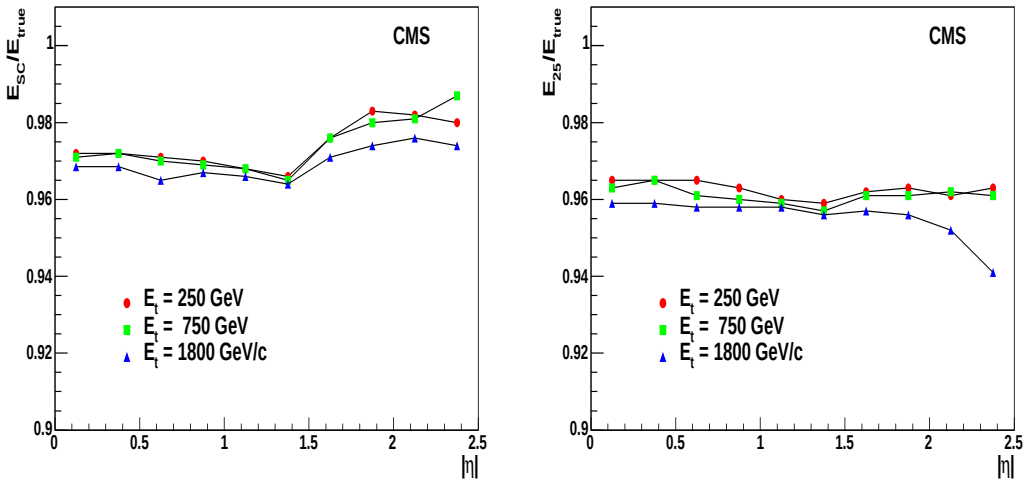

Figure 4: Dependence on η of the ratios $\mathrm{E_{SC}/E_{true}}$ (left) and $\mathrm{E_{25}/E_{true}}$(right).

Table 9: Position resolution: mean (μ) and sigma (σ) of gaussian fits.

$\mathrm{P_t}$ (TeV/c)	barrel		endcap	
	$\Delta\eta$ ($\times 10^3$)	$\Delta\phi$ (mrad)	$\Delta\eta$ $\times 10^3$	$\Delta\phi$ (mrad)
0.25	$\mu = 0.025$	$\mu = -0.11$	$\mu = -0.009$	$\mu = -0.006$
	$\sigma = 1.25$	$\sigma = 0.99$	$\sigma = 1.95$	$\sigma = 1.0$
0.75	$\mu = 0.038$	$\mu = -0.091$	$\mu = -0.067$	$\mu = -0.013$
	$\sigma = 1.16$	$\sigma = 0.78$	$\sigma = 1.80$	$\sigma = 0.80$
1.8	$\mu = -0.019$	$\mu = -0.088$	$\mu = 0.073$	$\mu = 0.015$
	$\sigma = 1.39$	$\sigma = 0.74$	$\sigma = 1.81$	$\sigma = 0.79$

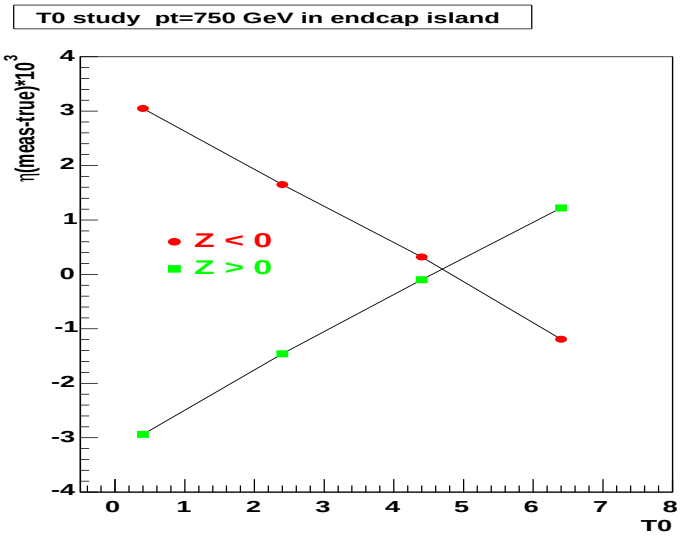

Figure 5: Tuning of T0 parameter for P_t=0.75 TeV/c.

The corresponding parameters are given in Table 10. From the effective widths is shown that the same performances are valid in a wide dynamic range P_t = 0.25 and 0.75 TeV/c, but become poorer at P_t=1.8 TeV/c.

To disentangle barrel and endcaps performances, examples of fits are shown respectively in Fig. 7 and in Fig. 8. It is clear that for the endcaps the resolution is better when taking Super-Clusters compared to 5×5 array matrix.

For the barrel and endcap energy resolutions, the gaussian fit σ and σ_{eff} are given in Table 11 and in Table 12 for the various samples studied.

3.3 Photon Cluster reconstruction

The two Super-Clusters are built to recover the energy deposited by converted photons that spread over a crystal matrix greater than 5×5. The energy loss in the preshower is taken into account for endcap Super-Cluster reconstruction. A correction based on the fraction (H/E) of the Super-Cluster energy measured in the hadron calorimeter (HCAL) is applied to correct for the small energy loss from shower leakage beyond the ECAL.

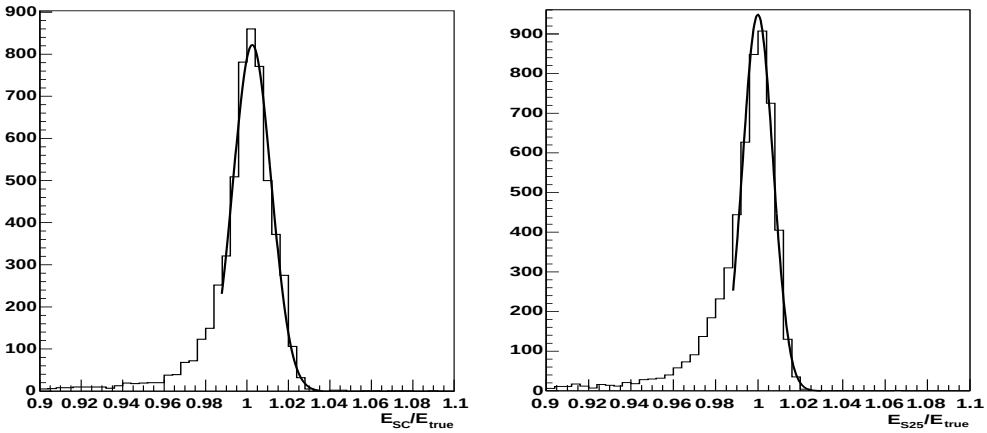

Figure 6: E_{SC}/E_{true} and E_{25}/E_{true} for E_T = 0.75 TeV/c photons.

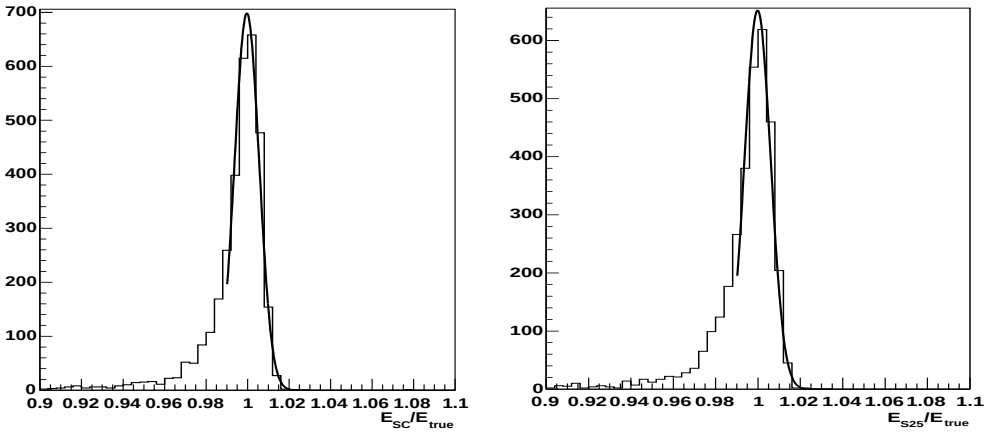

Figure 7: $\mathrm{E_{SC}/E_{true}}$ (left) and $E_{25}/\mathrm{E_{true}}$ (right) for $\mathrm{P_t}$ = 0.75 TeV$/c$ photons in the barrel.

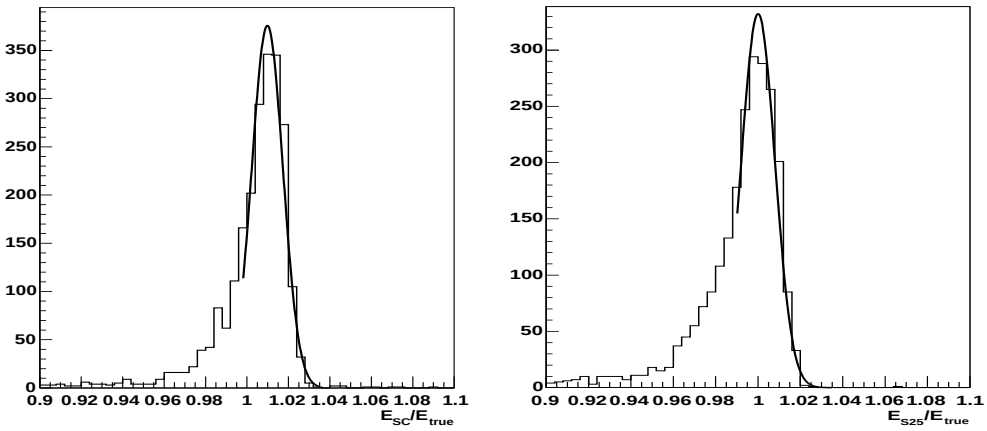

Figure 8: $\mathrm{E_{SC}/E_{true}}$ (left) and $E_{25}/\mathrm{E_{true}}$ (right) for $\mathrm{P_t}$ = 0.75 TeV$/c$ photons in the endcaps.

Table 10: Energy resolutions: mean μ and sigma σ of gaussian fits and σ_{eff}.

	E_{SC}/E_{true}			E_{25}/E_{true}		
P_t (TeV/c)	μ	σ	σ_{eff}	μ	σ	σ_{eff}
0.25	1.0	0.96%	1.20 %	0.994	0.92 %	1.43 %
0.75	1.00	0.92 %	1.16 %	1.00	0.72 %	1.25 %
1.8	0.993	1.09 %	1.59 %	0.989	0.87 %	1.63 %

Table 11: Energy resolutions: mean μ and sigma σ of gaussian fits and σ_{eff} in the barrel.

	E_{SC}/E_{true}			E_{25}/E_{true}		
P_t (TeV/c)	μ	σ	σ_{eff}	μ	σ	σ_{eff}
0.25	0.995	0.57%	0.89 %	0.996	0.57 %	0.81 %
0.75	1.00	0.59 %	0.89 %	1.00	0.62 %	1.0 %
1.8	0.991	0.63 %	1.24 %	0.999	0.67 %	1.27 %

Photon energy corrections are done in a simple way so far. For photons which deposit less than 1.7 TeV in the struck crytal (E_1) (most energetic one), a few per cent dependence on η of the ratio of the measured Super-Cluster energy E_{SC} to the generated energy E_{true} has been corrected for. The correction has been determined as in [8] from single photon samples at p_t = 0.25, 0.75 and 1.8 TeV/c. In the barrel the small effect (0.6%) comes from the geometry of the calorimeter. For very energetic photons, which deposit more than 1.7 TeV in crystal (E_1), saturation occurs in the barrel ECAL electronics because of the limited dynamical range of the multi-gain-pre-amplifier [16]. In the endcaps the saturation occurs at 3.0 TeV, which is beyond the reach of the present study. A simple correction of the energy (E_1) [8] measured in the most energetic crystal was applied based on the linear correlation between (E_1) and the energy deposited in the least energetic corner of 5 crystals ($E_5 = E_9 - E_4$, where E_9 and E_4 are the energies in the most energetic 3× 3 and 2 × 2 crystal arrays). A fit restricted to low energy data (in absence of saturation) is performed. Restricting the range of $20 < E_5 < 100$ GeV gives $E_1 = 12.6\ E_5$ [17]. The energy resolution after correction is $\sim$ 13% for the E_{25} reconstructed energy for 3-4 TeV/c^2 photons and considering only saturated events. It has to be noticed that in the present analysis, the graviton mass considered is $M_G \leq 4.5\mathrm{TeV}/c^2$, leading always to a very small fraction of saturated events.

3.4 Event selection

The events must satisfy the trigger conditions (Section 3.1). Each Super-Cluster must have E_t greater than 150 GeV and the two Super-Clusters with the highest E_t are selected as photon candidates. The main reducible backgrounds at this level are due to QCD jet-jet, γ-jet and Drell-Yan events. The selection cuts, listed below, are based on the reconstruction of two very energetic and isolated photons in the final state.

- In order to reduce the background coming from jets, the two Super-Clusters must be isolated in the electromagnetic calorimeter. The isolation criterion is based on the sum of the transverse energies deposited in clusters within a cone of opening radius $\Delta R = \sqrt{(\Delta\eta)^2 + (\Delta\phi)^2}$ centred around and excluding the photon candidate. The photon candidate is isolated if, in a cone of $\Delta R < 0.5$, the sum is below 2 % of the transverse energy of the Super-Cluster. This cut has an efficiency of 84.8 % for a 1.5 TeV/c graviton mass (Table 13 and Fig. 9).
- The background from hadrons is eliminated with a cut on the hadronic energy fraction (H/E). The condition $H/E < 0.05$ keeps a signal efficiency of 99.2 % while giving a rejection factor of 4.6 and 28.3 for

Table 12: Energy resolutions: mean μ and sigma σ of gaussian fits and σ_{eff} in the endcaps.

	E_{SC}/E_{true}			E_{25}/E_{true}		
P_t (TeV/c)	μ	σ	σ_{eff}	μ	σ	σ_{eff}
0.25	1.0	0.82%	1.15 %	0.994	0.96 %	1.2 %
0.75	1.00	0.75 %	1.20 %	1.00	0.79 %	1.4 %
1.8	0.993	1.04 %	1.76 %	0.985	1.33 %	2.26 %

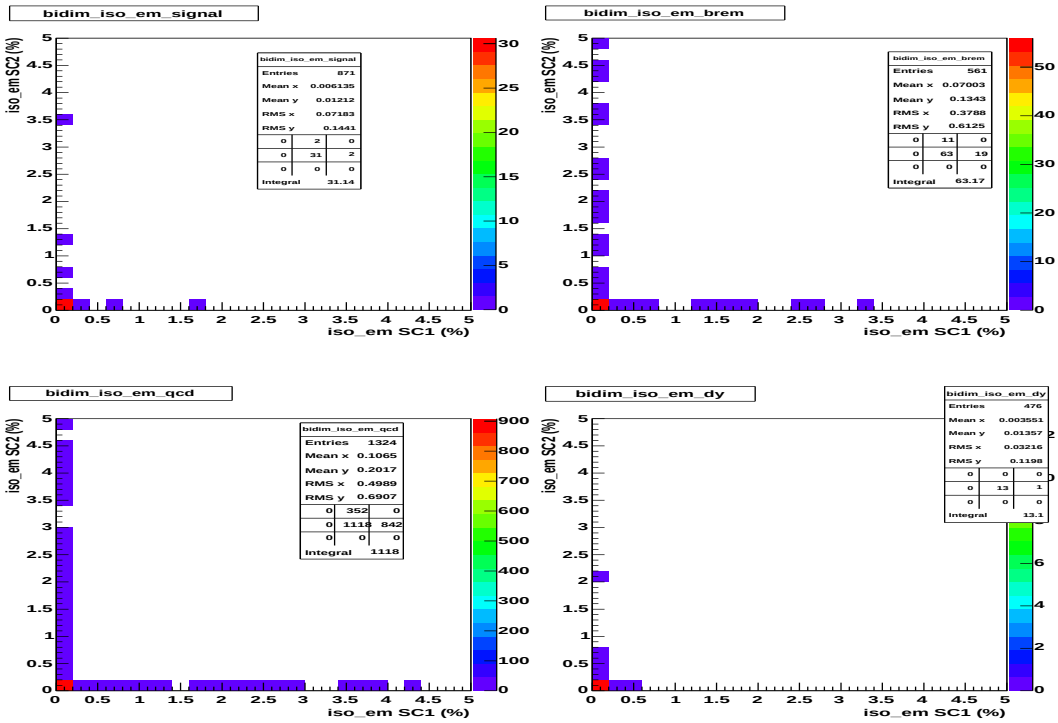

Figure 9: 2D plot of the sum of the transverse energies deposited in clusters within a cone of opening radius $\Delta R < 0.5$ centred around and excluding the first most energetic Super-Cluster divided by the energy of the first most energetic Super-Cluster, vs the same ratio for the second most energetic Super-Cluster, for the signal 1.5 TeV/c^2 graviton (top-left), γ-jet (top-right), QCD (bottom-left) and Drell-Yan (bottom-right) in 1.4 TeV/c^2-1.6 TeV/c^2 mass range.

respectively γ-jet and QCD background events (Table 13 and Fig. 10).

- To further reduce these backgrounds, tracker isolation is required: the sum of the tranverse energies of the charged particle tracks deposited in a cone ΔR = 0.5 around the Super-Cluster should be below 1 % of the transverse energy of the Super-Cluster. It rejects γ-jet by an additional factor 26 while killing remaining PYTHIA QCD background (Table 13 and Fig. 11).

The huge γ-jet and QCD backgrounds are efficiently rejected by these cuts. The only relevant background is formed by the photon pairs from quark annihilation.

4 K-factors

To produce the final results and to calculate the expected statistical significance for RS graviton search recently calculated next-to-leading order corrections (K factors) to the cross-sections of different types of background are used:

- Signal: K factor = 1
- Quark annihilation [18]: K factor = 1.5
- Gluon fusion [19]: K factor = 1.2
- γ + hadronic jets [19] : K factor = 1 for the purposes of our study
- QCD hadronic jets: K factor = 1

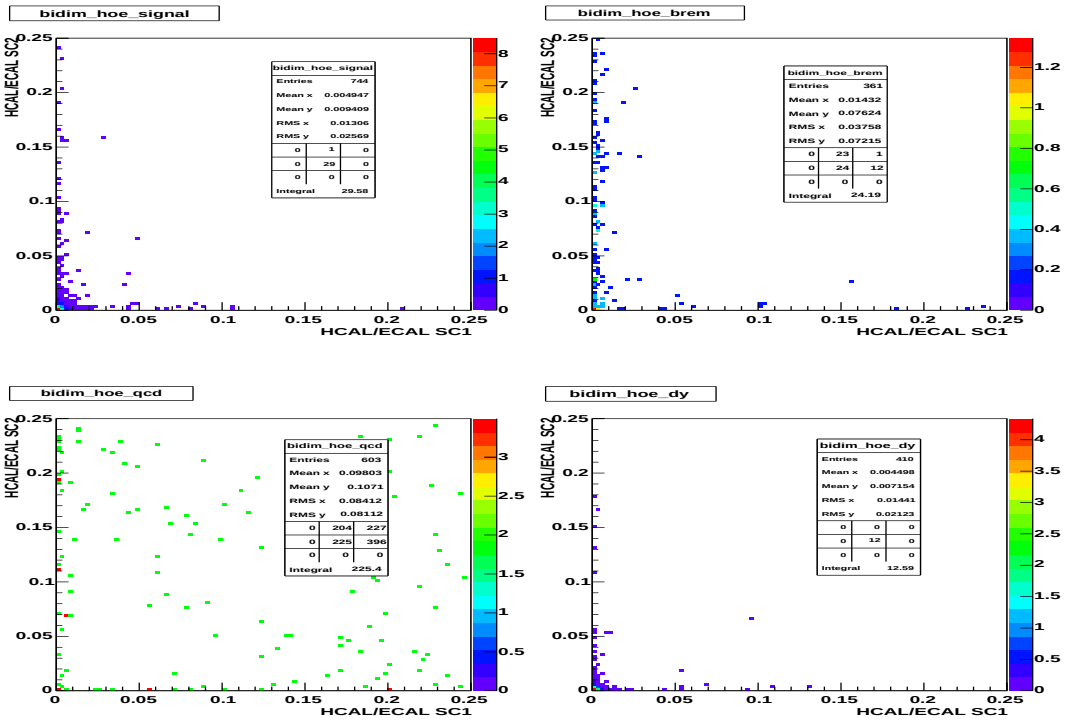

Figure 10: 2D plot of the E_{HCAL}/E_{ECAL} ratio for the first most energetic supercluster vs E_{HCAL}/E_{ECAL} for the second most energetic super cluster, for the signal 1.5 TeV/c^2 graviton (top-left), γ-jet (top-right), QCD (bottom-left) and Drell-Yan (bottom-right) in 1.4 TeV/c^2- 1.6 TeV/c^2 mass range.

5 Results

The graviton invariant mass is reconstructed from the two Super-Clusters. For each value of the generated graviton mass, the corresponding peak is fitted to a Gaussian distribution. The σ of the fit is $\simeq$ 10 GeV/c^2 for M_G = 1.5 TeV/c^2 and c=0.01 (Fig. 12), reflecting the detector energy resolution, which is slightly below 0.5% constant term, as obtained from 2004 test beam data; and an additional contribution of 0.16% which is due to the reconstruction.

For M_G = 3.5 TeV/c^2 and c=0.1 it increases up to $\simeq$ 35 GeV/c^2, due to the natural width of the resonance. As an example, the σ of the fit is $\simeq$ 35 GeV/c^2 for M_G = 3.0 TeV/c^2 and c=0.075 (Fig. 12) reflects the natural width of the resonance.

A $\pm 3\sigma$ window is defined around the fitted peak to compute the numbers of signal and background events, N_s and N_{bkg}. The corresponding number of events, obtained through the successive analysis cuts described above are given for an integrated luminosity $\mathcal{L}$ = 30 fb^{-1} in Table 13 for (M_G = 1.5 TeV/c^2, c = 0.01) and in Table 14 for (M_G = 3.5 TeV/c^2, c = 0.1).

Table 13: Number of events passed through the analysis cuts described in Section 3.4 for M_G = 1.5 TeV/c^2, c = 0.01 and $\mathcal{L}$= 30 fb^{-1}. Leading column is non-saturated events, all saturated events, passed through the analysis, were added in brackets, where applied.

	signal	Born (k=1.5)	Box (k=1.2)	Brem (k=1)	QCD (k=1)	DY (k=1)
trigger + 2SC	28.9	8.6	0.10	29.2	798.7	4.3
+ EM isolation	24.5	5.5	0.08	20.3	361.8	3.5
+ H/E	24.3	5.4	0.08	4.4	12.8	3.5
+ tracker isolation	17.6	4.2(+0.2)	0.05	0.17	0.0	0.0

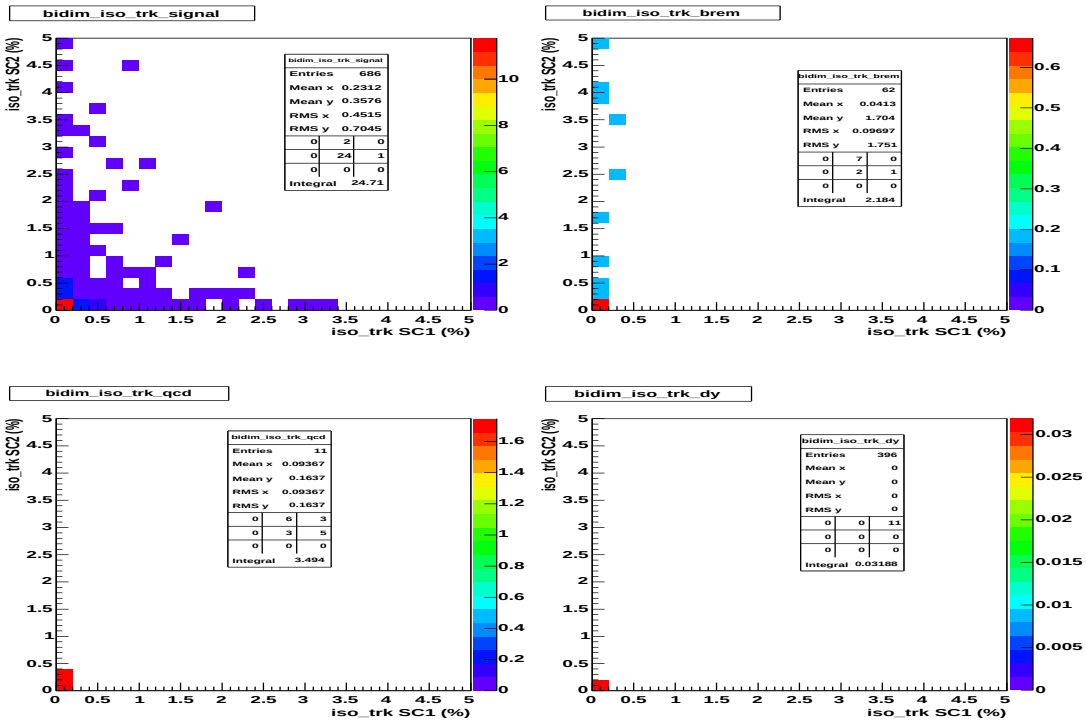

Figure 11: 2D plot of the charged particles with a tracks, deposited in a cone ΔR = 0.5 around the Super-Cluster, divided by the energy of this Super-Cluster, vs the same ratio for the second most energetic Super-Cluster, for the signal 1.5 TeV/c^2 graviton (top-left), γ-jet (top-right), QCD (bottom-left) and Drell-Yan (bottom-right) in 1.4 TeV/c^2-1.6 TeV/c^2 mass range.

Table 14: Number of events passed through the analysis cuts defined above for $M_G = 3.5$ TeV/c^2, $c = 0.1$ and $\mathcal{L}$ = 30 fb^{-1}. Leading column is non-saturated events, all saturated events, passed through the analysis, were added in brackets, where applied.

	signal	Born (k=1.5)	Box (k=1.2)	Brem (k=1)	QCD (k=1)	DY (k=1)
trigger + 2SC	11.6	0.20	$4.4 * 10^{-4}$	0.78	821.9	0.10
+ EM isolation	10.8	0.14	$3.6 * 10^{-4}$	0.32	164.4	$9.5 * 10^{-2}$
+ H/E	10.6	0.13	$3.4 * 10^{-4}$	$1.6 * 10^{-2}$	0.0	$9.5 * 10^{-2}$
+ tracker isolation	8.9(+1.0)	0.10(+0.02)	$2.7(+0.24) * 10^{-4}$	$1.7 * 10^{-3}$	0.0	$7.2 * 10^{-4}$

Signals over backgrounds with all events satisfying all the selection cuts (Section 3.4) are displayed in Fig. 13 for ($M_G = 1.5$ TeV/c^2, $c = 0.01$), ($M_G = 3.0$ TeV/c^2, $c = 0.1$) and for an integrated luminosity of 30 fb^{-1}. In Fig. 14, signal over backgrounds are given for ($M_G = 1.0$ TeV/c^2, $c = 0.01$), ($M_G = 2.5$ TeV/c^2, $c = 0.1$) and for an integrated luminosity of 10 fb^{-1}.

Taking into account K-factors described above, the number of expected signal and background events, N_s and N_{bkg} respectively, are computed. The significance is evaluated, for different masses for $c = 0.01$ and $c = 0.1$ and $\mathcal{L}$ = 30 fb^{-1} with the Poisson statistics counting method: $S_{L2} = \sqrt{2lnQ}$ with:

$$Q = (1 + \frac{N_s}{N_{bkg}})^{N_s + N_{bkg}} \exp(-N_s). \quad (1)$$

Expected statistical significance S_{L2} is plotted for (M_G, c) space for 10 fb^{-1}, 30 fb^{-1} and 60 fb^{-1} (Fig. 15). Uncertainties were not taken into account on Fig. 15.

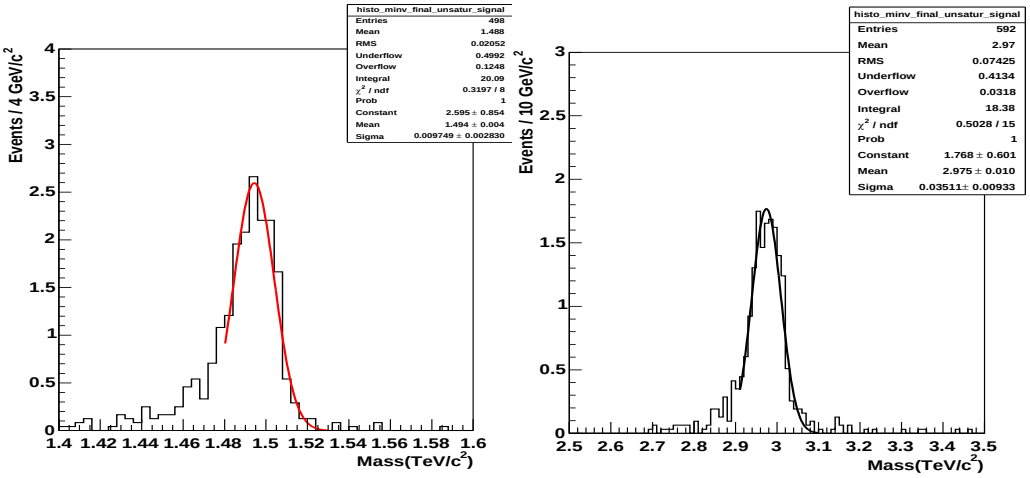

Figure 12: The σ of the fit is $\simeq$ 10 GeV/c^2 for M_G = 1.5 TeV/c^2 and c=0.01 (left) which reflected the detector energy resolution. The σ of the fit is $\simeq$ 35 GeV/c^2 for M_G = 3.0 TeV/c^2 and c=0.075 (right) which reflected the natural width of the resonance.

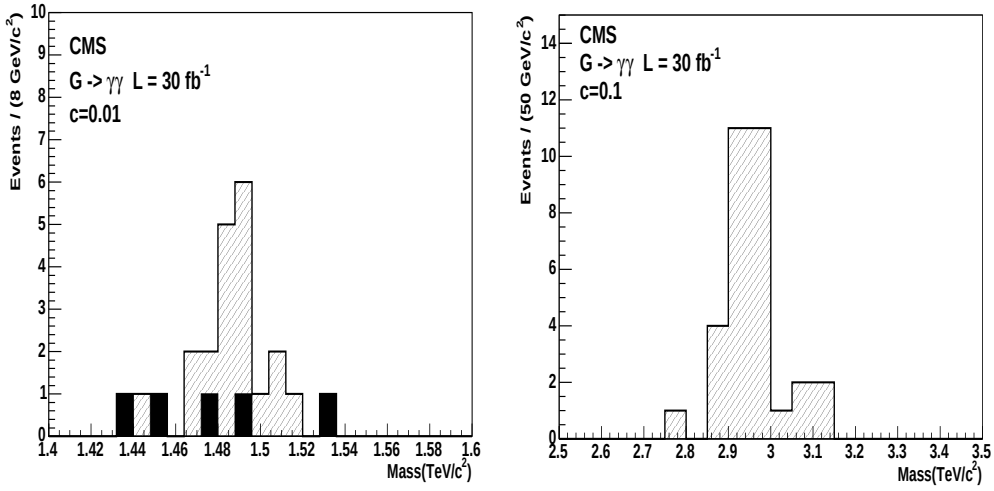

Figure 13: Number of events passed through all cuts for (M_G = 1.5 TeV/c^2, c = 0.01) (left) and (M_G = 3.0 TeV/c^2, c = 0.1) (right) RS-1 gravitons for 30 fb^{-1} integrated luminosity. Dashed and black histograms correspond respectively to signal and bakground.

Table 15: Significance for $c = 0.01$ and $\mathcal{L} = 30 fb^{-1}$.

	$M_G = 1.0$ TeV/c^2	$M_G = 1.25$ TeV/c^2	$M_G = 1.5$ TeV/c^2	$M_G = 1.75$ TeV/c^2	$M_G = 2.0$ TeV/c^2
N_s	135.8	44.0	17.6	7.3	3.9
N_{bkg}	15.0	8.8	4.6	1.8	1.2
S_{L2}	20.6	10.1	5.9	3.9	2.6

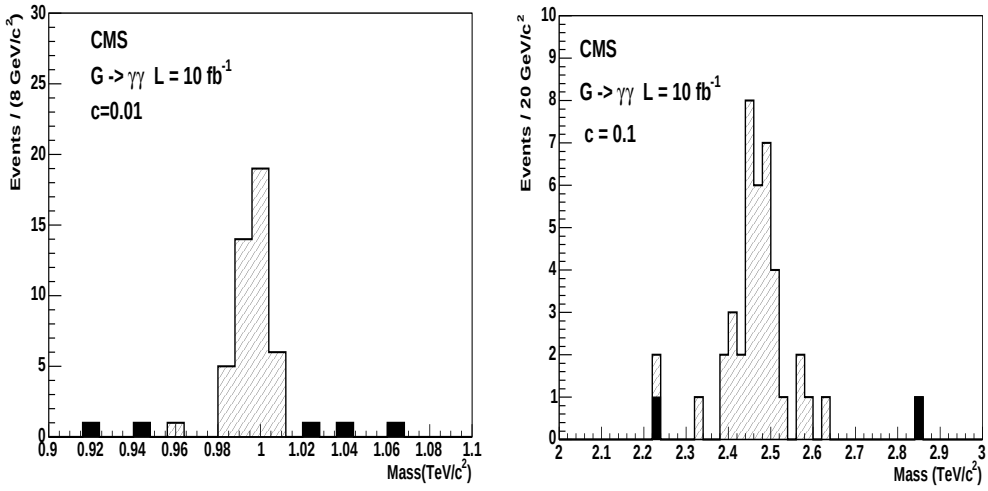

Figure 14: Number of events passed through all cuts for ($M_G = 1$ TeV$/c^2$, $c = 0.01$) (left) and ($M_G = 2.5$ TeV$/c^2$, $c = 0.1$) (right) RS-1 gravitons for an integrated luminosity of 10 fb^{-1}. Dashed and black histograms correspond respectively to signal and background.

Table 16: Significance for $c = 0.1$ and $\mathcal{L}$= 30 fb^{-1}.

	$M_G = 2.5$ TeV$/c^2$	$M_G = 3.0$ TeV$/c^2$	$M_G = 3.5$ TeV$/c^2$	$M_G = 4.0$ TeV$/c^2$	$M_G = 4.5$ TeV$/c^2$
N_s	103.8	31.6	9.9	3.44	1.11
N_{bkg}	1.11	0.35	0.13	0.06	0.02
S_{L2}	27.3	15.0	8,2	4.6	2.6

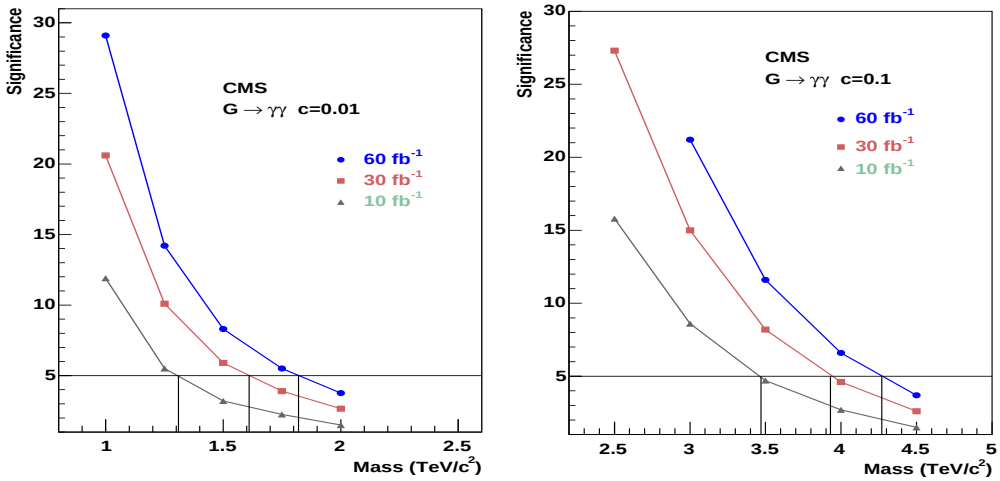

Figure 15: Expected statistical significance S_{L2} is plotted on (M_G, c) space for $\mathcal{L}$= 10 fb^{-1}, 30 fb^{-1} and 60 fb^{-1}. Left: $c = 0.01$, Right: $c = 0.1$.

Using S_{L2} for the expected significance, a 5σ discovery can be achieved:

- for $\mathcal{L}$ = 10 fb^{-1}:
  - $c = 0.01$ $M_G = 1.31$ TeV$/c^2$
  - $c = 0.1$ $M_G = 3.47$ TeV$/c^2$
- for $\mathcal{L}$ = 30 fb^{-1}:
  - $c = 0.01$ $M_G = 1.61$ TeV$/c^2$
  - $c = 0.1$ $M_G = 3.95$ TeV$/c^2$
- for $\mathcal{L}$ = 60 fb^{-1}:
  - $c = 0.01$ $M_G = 1.82$ TeV$/c^2$
  - $c = 0.1$ $M_G = 4.27$ TeV$/c^2$

The discovery region in the plane of the coupling parameter c and the graviton mass is given in Fig. 16.

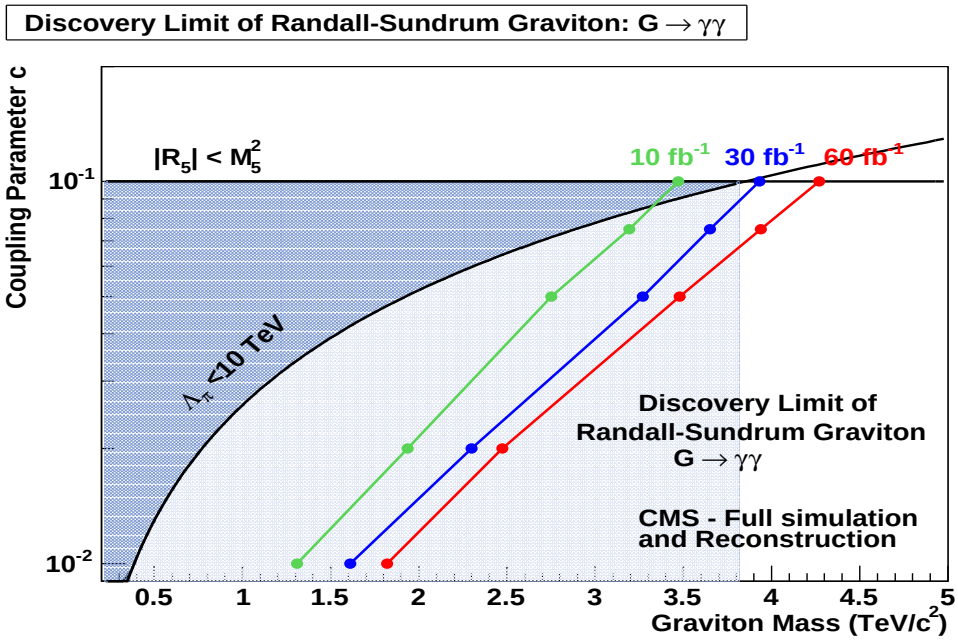

Figure 16: Reach of the CMS experiment in the search for the Randall-Sundrum graviton decaying into diphoton channel as a function of the coupling parameter c and the graviton mass for $\mathcal{L}$ = 10, 30 and 60 fb^{-1}. The left part of each curve is the region where the significance exceeds 5σ. The shaded part corresponds to the condition $\Lambda_\pi \leq 10$ TeV which is theoritically preferred [4].

The comparison of discovery regions for the Randall-Sundrum graviton decaying into diphoton as well as into electron channels as a function of the coupling parameter c and the graviton mass for $\mathcal{L}$ = 10 and 30 fb^{-1} in the plane of the coupling parameter c and the graviton mass is given in Fig. 17 (significance for the electron case was recalculated based on S_{L2} estimator to be able to compare our results. The shaded part corresponds to the condition $\Lambda_\pi \leq 10$ TeV which is theoritically preferred [4]).

6 Cross-section uncertainties

6.1 Hard process scale

Usually, the hard process defines the Q^2 scale, which directly influences the parametrization of PDF structure functions and α_s which, in turn, influences the cross-section.

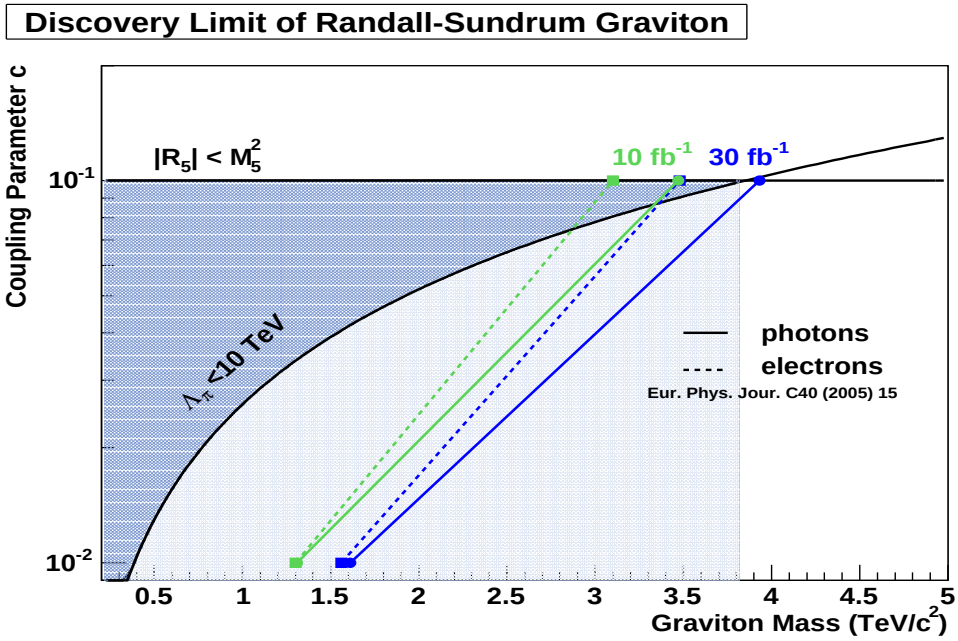

Figure 17: Reach of the CMS experiment in the search for the Randall-Sundrum graviton decaying into diphoton and electron channels as a function of the coupling parameter c and the graviton mass for $\mathcal{L}$ = 10 and 30 fb^{-1}. The left part of each curve is the region where the significance exceeds 5σ.

The dependence of the observables on the choice of the Q^2 scale is unphysical and should be treated as one of the contributions to the total uncertainty of the theoretical predictions.

The usual choice for the hard process scale in $2 \to 1$ processes is often $\hat{s}$, which is the default in PYTHIA. In order to study the effect of the hard process scale variation for $2 \to 1$ processes, two scenarious were used, corresponding to $0.25\hat{s}$ and $4.0\hat{s}$ [20]. Results for the most important background and signals are presented in Table 17.

Table 17: Hard scale uncertainties for the selected signal datasets as well as for selected background datasets.

c=0.01	1.25 TeV/c^2	1.5 TeV/c^2	1.75 TeV/c^2
$4\hat{s}$	-8.3%	-8.2%	-8.9%
$0.25\hat{s}$	+8.7%	+10.7%	+10.3%
c=0.1	3.5 TeV/c^2	4.0TeV/c^2	4.5TeV/c^2
$4\hat{s}$	-10.2%	-12.7%	-12.3%
$0.25\hat{s}$	+12.5%	+13.9%	+14.2%
born	1300-1900, GeV/c^2 CKIN(1)-CKIN(2)	1900-3200, GeV/c^2 CKIN(1)-CKIN(2)	3200-5250, GeV/c^2 CKIN(1)-CKIN(2)
$4\hat{s}$	-0.26%	+0.59%	-0.49%
$0.25\hat{s}$	+0.68%	+0.18%	+2.55%

Hard scale confidence limits uncertainties for 30 fb^{-1} can be found in Table 18.

6.2 PDF uncertanties

The parton distribution functions of interacting particles describe the probability density for partons undergoing hard scattering at the hard process scale Q^2 and taking a certain fraction x of the total particle momentum.

Various approaches are currently available to quote the PDFs of the proton, but CTEQ6M and MRST PDFs seem to be well suited for use in Monte Carlo simulations for the LHC [20] (see also Appendix A).

ΔX_C estimator of PDF uncertainties (see Appendix A) will be used to estimate the cross-section uncertainties in this analysis.

Table 18: Hard scale confidence limits uncertainties for 30 fb^{-1}.

	$4\hat{s}$	$0.25\hat{s}$
$c = 0.01$	-62 GeV/c^2	+56 GeV/c^2
$c = 0.1$	-47 GeV/c^2	+42 GeV/c^2

Table 19: PDF uncertainties for the selected signal datasets as well as for selected background datasets.

c=0.01	1.25 TeV/c^2	1.5 TeV/c^2	1.75 TeV/c^2
CTEQ6M, $\Delta X_C/X_0$	8.3%	8.6%	11.7%
c=0.1	3.5 TeV/c^2	4.0TeV/c^2	4.5TeV/c^2
CTEQ6M, $\Delta X_C/X_0$	23.3%	25.7%	30.8%
born	1300-1900, GeV/c^2 CKIN(1)-CKIN(2)	1900-3200, GeV/c^2 CKIN(1)-CKIN(2)	3200-5250, GeV/c^2 CKIN(1)-CKIN(2)
CTEQ6M, $\Delta X_C/X_0$	6.15%	6.24%	11.44%

PDF confidence limits uncertainties for 30 fb^{-1} are:

- $c = 0.01$, -55GeV/c^2
- $c = 0.1$, -152GeV/c^2

6.3 Other uncertainties

There are three other sources of uncertainties:

1) K-factors 1.5 and 1.2 were used for born and box subprocesses during the significance calculations. If K-factors equal to 1 will be used for these subprocesses, confidence limits will move:
   - $c = 0.01$, $+70$GeV/c^2
   - $c = 0.1$, $+40$GeV/c^2
2) There is another source of uncertainties due to the fact that K-factor = 1.5 has been used for born process, while Tevatron most recent measurements pointed out that this K-factor is closer to 2 [23]:
   - $c = 0.01$, -50GeV/c^2
   - $c = 0.1$, -30GeV/c^2
3) Including preselection inefficiency (see Sect. 2) confidence limits uncertainties would be
   - $c = 0.01$, -8GeV/c^2
   - $c = 0.1$, -5GeV/c^2

7 Conclusions

This note presents the study of Randall-Sundrum graviton excitations decaying into two photons with full simulation and reconstruction. With a 30 fb^{-1} integrated luminosity, a 5 σ discovery can be reached up to 1.61 TeV/c^2 for low coupling c = 0.01, and 3.95 TeV/c^2 for high coupling c = 0.1. Systematic uncertainties on cross-sections from QCD scale and LHAPDF proton parton distributions have been estimated.

8 Acknowledgments

In the preparation of this note we benefited greatly from discussions with PRS SUSYBSM group, PRS egamma group and referees. We would like to express our sincere thanks to Luc Pape, Maria Spiropulu, Sergei Slabospitsky, Rick Cavanaugh and Reyes Alemany Fernandez.

9 Appendix A

The LHAGLUE interface [21] included from the most recent LHAPDF versions simplifies the use of the Les Houches accord PDF in PYTHIA by the switches $MSTP(52) = 2$, $MSTP(51) = LHAPDF_{id}$, where $LHAPDF_{id}$ is documented in [22].

There are 40 fits for CTEQ6M with $MSTP(51) = 10050$ is equivalent for the main fit and $MSTP(51) = 10051 - 10090$ for 40 additional weights. Lets X(S) be any variable which depends on PDFs. We are calculating the PDF "best fit", $X_0 = X(S_0)$, and the rest of the fits $X_k^{\pm} = X(S_k^{\pm})$, where

$$D_k = X_k^+ - X_k^-, k = 1, ..., d, \quad D_k = (X_k^+ - X_0) - (X_k^- - X_0)$$

$$R_j, j = 1, ..., 2d, \quad R_1 = X_1^+ - X_0, R_2 = X_1^{-1} - X_0, R_3 = X_2^+ - X_0, R_4 = X_2^- - X_0, ...$$

There are two major equations to calculate uncertainties [20]:

$$\Delta X = \frac{1}{2}\sqrt{\sum_{i=1}^{N_{PDF}} [X_{2i} - X_{2i-1}]^2}, \qquad \Delta X_C = \frac{1}{2}\sqrt{\sum_{i=1}^{2N_{PDF}} [X_i - X_0]^2}$$

References

[1] N. Arkani-Hamed, S. Dimopoulos, G.Dvali, Phys. Lett. **B249** (1998) 263
I. Antoniadis, N. Arkani-Hamed, S. Dimopoulos, G.Dvali, Phys. Lett. **B436** (1998) 257

[2] L. Randall, R. Sundrum, Phys. Rev. Lett. **83** (1999) 3370 and *ibid* (1999) 4690.

[3] I. Antoniadis, Phys. Lett. **B246** (1990) 377
I. Antoniadis, C. Munoz, M.Quiros, Nucl. Phys. **B397** (1993) 525
I. Antoniadis, K. Benalki, Phys. Lett. **B236** (1994) 69

[4] H.Davoudiasl, J.L. Hewett and T.G. Rizzo, *"Experimental Probes of Localized Gravity: On and Off the Wall"*, Phys. Rev. **D63** (2001) 075004.

[5] D0 Collaboration, V.M. Abazov et al., *"Search for Randall-Sundrum Gravitons in Dilepton and Diphoton Final States"*, hep-ex/0505018.

[6] T. Pratt and R. Culbertson, *"Analysis of High Mass Di-Photon Events and Search for Randall-Sundrum Gravitons"*, $http://www-cdf.fnal.gov/physiscs/exotic/r2A/20040805.diphoton_rsgrav$.

[7] G. Landsberg, *"Collider Searches for Extra Dimensions"*, SLAC Summer Institute on Particle Physics (SSI04), Aug. 2-13,2004.

[8] C. Collard and M.-C. Lemaire,*"Search with the CMS detector for Randall-Sundrum excitations of gravitons decaying into electron pairs"*, **Eur. Phys. Jour. C40, Supp 1, (2005) 15**.

[9] T. Sjöstrand, Comput. Phys. Commun. **82** (1994) 74;
T. Sjöstrand et al., Comput. Phys. Commun. **135** (2001) 238, LU TP 00-30, hep-ph/0010017.

[10] CTEQ Collaboration, H.L. Lai et al., *"Global QCD Analysis of Parton Structure of the Nucleon: CTEQ5 Parton Distributions"*, Eur. Phys. J. **C12** (2000) 375.

[11] CMS Collaboration, **CERN/LHCC 2000-038, CMS TDR 6.1**, *"CMS The Tridas Project Design Report, Volume 1: The Trigger Systems"*.

[12] CMS Collaboration, **CERN/LHCC 2002-02, CMS TDR 6.2**,*"CMS The Tridas Project Technical Design Repor t, Volume 2:Data acquisition and High-Level Trigger"*.

[13] CMS Collaboration, "*Object oriented Simulation for CMS Analysis and Reconstruction"*,
http://cmsdoc.cern.ch/oscar/.

[14] CMS Collaboration, *"CMS OO Reconstruction"*,
http://cmsdoc.cern.ch/orca/.

[15] E. Meschi, T. Montero, C. Seez and P. Vikas, *"Electron Reconstruction in the CMS Electromagnetic Calorimeter"*, **CMS NOTE 2001-034**.

[16] M. Raymond, J. Crooks, M. French and G. Hall, *"The MGPA Electronic Calorimerer Readout Chip for CMS"*, Proceeding of the 2003 LECC Conference, **CERN-2003-006**.

[17] B. Clerbaux, T. Mahmoud, C. Collard, M.-C. Lemaire and V. Litvin, *"TeV electron and photon saturation studies"*, CMS Note 2006/004.

[18] T. Binoth *et al.*, QCD/SM Working Group, Les Houches, 2001.

[19] Z. Bern, L. Dixon, C. Schmidt, Phys. Rev. **D 66** (2002) 074018.

[20] P. Bartalini, R.Chierici, A De Roeck, "Guidelines for the estimation of theoretical uncertainties at the LHC", CMS Note 2005/013, 2005.

[21] D.Bourilkov, [hep-ph 0508110]

[22] H. Baer et al [hep-ph 0403045]. Code and documentation available at *http://durpdg.dur.ac.uk/lhapdf*

[23] D. Acosta et al, CDF Collaboration, **PRL 95 (2005) 022003**, 2005.